HEAT TRANSFER, FLOW PATTERNS, AND RESULTING STRATIFICATION IN TWO DIMENSIONAL VERTICAL CONVECTION: A SYSTEMATIC STUDY

Martin Goxe
Autorité de Sûreté Nucléaire et
Radioprotection (ASNR), PSN-RES
Aix Marseille Univ,CNRS,Centrale Marseille
IRPHE
martin.goxe@asnr.fr

Michael Le Bars
Aix Marseille Univ,CNRS,Centrale Marseille
IRPHE
michael.le-bars@univ-amu.fr

Julie-Anne Zambaux
Autorité de Sûreté Nucléaire et Radioprotection
(ASNR), PSN-RES
julie-anne.zambaux@asnr.fr

ABSTRACT

For vertical natural convection in a differentially heated two-dimensional rectangular cavity, the impact of a high aspect ratio (cavity height over its width), $\Gamma = 5$ is investigated. on the flow regimes and heat transfer characteristics in turbulent vertical convection. Using direct numerical simulations (DNS), we explore the transitions between regimes across a wide range of Rayleigh numbers ($10^8 \leq Ra \leq 10^{14}$), focusing on the evolution of the central stratification S, Nusselt number Nu, and Reynolds number Re.

Our results confirm the persistence of the three regimes in the $\Gamma = 5$ configuration, with the first transition occurring at critical Rayleigh numbers comparable to the $\Gamma = 1$ case (Wang *et al.*, 2021*b*). However, key differences emerge in Regime II and the transition to Regime III. The overall evolution of the central stratification differs, as its maximum is reached earlier. On the other hand, scaling laws for Nu and Re remain consistent with the ones obtained for $\Gamma = 1$, suggesting that global heat transport and flow dynamics are robust to changes in aspect ratio. These findings provide new insights into the interplay between geometry and turbulence, relevant in industrial configuration such as cooling pools.

As we reach a critical Rayleigh number, the displacement boundary layer thickens due to turbulent structures, deviating from the classical $Ra^{-1/4}$ scaling. The thermal boundary layer, conversely, remains unaffected by turbulence for $Pr > 1$, adhering to theoretical predictions. Vertical velocity profiles reveal a shift in the location of the maximum velocity toward the walls, accompanied by a reduction in amplitude as kinetic energy dissipates into turbulent structures.

INTRODUCTION

Due to an increasing demand for de-carbonized and affordable energy, new smaller nuclear power plants designs are being developped. Several of these Small Modular Reactors (SMR) propose to immerse the reactor containment in water-filled pool, to remove residual heat under both normal and accidental operating conditions (De Angelis *et al.*, 2023). In accidental scenarios, the relatively large temperature difference between the cold water pool and inside the reactor containment wall, combined with the characteristic height of the system ($\approx$ 10 m), induces a strongly turbulent natural convection regime (height-based Rayleigh number Ra $\approx 10^{14}$). The appropriate heat-transfer correlations for such high-Rayleigh-number flows are still under debate, yet they are crucial for accurately predicting the accident evolution. The present work addresses the problem of vertical natural convection using a representative configuration: the differentially heated cavity (DHC). This configuration has been extensively investigated in the low-Rayleigh, laminar regime, where robust Nusselt (Nu) correlations and analytical description of the vertical boundary layers have been established by (Batchelor, 1954). The onset of turbulence has also been examined, and critical Rayleigh numbers have been reported for various fluids, including water and air. Prandtl number was identified as a key parameter governing both the transition process and the resulting flow organization (Khoubani *et al.*, 2024). Industrial applications, such as ventilation and related thermal management systems in air, have driven research on moderate to high Rayleigh numbers : Ra $\approx 10^{11} - 10^{12}$ (Sergent *et al.* (2013*b*) ; Trias *et al.* (2010)), for which experimental data and numerical simulations have been compared. However, discrepancies persist in the prediction of the central thermal stratification, $S = \left.\frac{\partial T}{\partial z}\right|_{center}$, which remains a challenging aspect of the DHC problem. For high-Prandtl-number fluids (Pr $\approx$ 10), such as water, the available literature is more limited, even though the flow physics is expected to differ from that of low-Prandtl fluids, including beyond the transition to turbulence (Ke *et al.*, 2026). In particular, the work done by Wang *et al.* (2021*b*) reported the existence of three distinct regimes with increasing Rayleigh number in a 2D square cavity for $Pr = 10$. The first two regimes describe the flow organization before and immediately after the transition to turbulence in the boundary layers. The third regime corresponds to a fully mixed core, in which the central

stratification returns to nearly zero over a range of Rayleigh numbers ($10^{13} < Ra < 10^{14}$), consistent with those anticipated in SMR cooling pools.
Another important parameter identified in the literature is the aspect ratio, $\Gamma = H/L$ (with H the height of the cavity and L its length). It has been shown to influence the flow structure in both laminar (Wang *et al.*, 2021*a*) and turbulent regimes (Khoubani *et al.*, 2024), predominantly in air. Its effect in the turbulent flow of high-Prandtl-number fluids such as water is still not clearly understood. As water pools in several SMR designs are planned to have a rather large aspect ratio (De Angelis *et al.*, 2023), it is of interest to study how the three regimes identified and corresponding flow structures are impacted when this ratio increases. In the current study, an aspect ratio of $\Gamma = 5$ has been considered.

NUMERICAL METHODS

We consider a two-dimensional rectangular DHC configuration with an aspect ratio $\Gamma = 5$, as illustrated in figure 1, and investigate Rayleigh numbers in the range 10^7–10^{14}. Here, the height-based Rayleigh number is defined as $Ra = (\alpha \Delta T g H)/(\nu\kappa)$, where α is thermal dilatation coefficient, $\Delta T = T_h - T_c$ the temperature difference between the two walls, g the gravity acceleration and ν, κ the kinematic viscosity and thermal diffusivity respectively. The left and right boundaries are isothermal walls, with $T_{wall} = T_h$ and $T_{wall} = T_c$, respectively, and a no-slip condition $\vec{u}_{wall} = 0$. The top and bottom boundaries are modeled as adiabatic, $\partial T/\partial z = 0$, with free-slip velocity conditions. Under the Oberbeck–Boussinesq approximation, the corresponding non-dimensional governing equations are given by:

$$\begin{cases} \nabla \cdot \vec{u} = 0 \\ \dfrac{\partial \vec{u}}{\partial t} + \vec{u} \cdot \nabla \vec{u} = -\nabla p + \sqrt{\dfrac{Pr}{Ra}} \nabla^2 \vec{u} + T \vec{e}_z \\ \dfrac{\partial T}{\partial t} + \vec{u} \cdot \nabla T = \dfrac{1}{\sqrt{PrRa}} \nabla^2 T \end{cases} \quad (1)$$

where $\vec{u}$, T, and p denote the non-dimensional velocity, temperature, and pressure, respectively. The reference quantities are the cavity height H and the free-fall velocity $u_{fall} = \sqrt{\alpha \Delta T g H}$.The Prandtl number is defined as $Pr = \nu/\kappa$.

As the domain geometry is rather simple, the pseudo-spectral code Dedalus (Burns *et al.*, 2020) is used for this study. The fields are expanded onto a Chebyshev basis in the x-direction and onto either a sine or cosine basis in the z-direction, thereby enforcing periodicity along the z-axis and enabling faster computations. To avoid issues for the gravity induced natural convection loop due to this periodicity condition in the vertical direction, the buoyancy term is set to zero within a four-mesh-layer region near the top and bottom boundaries. Tests using different boundary-layer thicknesses revealed no influence of this parametrization on the global flow.

The number of mode on each directions N_x, N_z reflects a trade-off between accurately capturing the smallest turbulent scales and managing computational cost. Since the Chebyshev basis naturally projects onto a Gauss–Lobatto distribution, expressed as $n_i = 1 + cos(\frac{i\pi}{N_x}) * \frac{1}{2\Gamma}$, $1 \leq n_i \leq N_x$, the resulting mesh is finer near the hot and cold walls. Consequently, the primary constraint was carried by N_z. Convergence tests

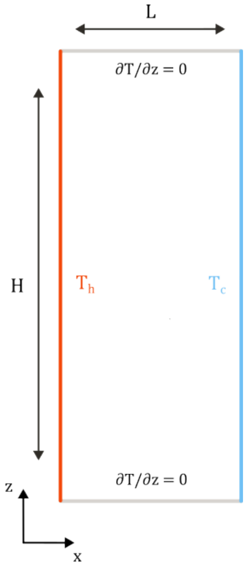

Figure 1. Sketch of two-dimensional vertical convection with large aspect ratio.

were conducted for two key configurations : $Ra = 5 \times 10^{11}$ ($N_x \times N_z = 256 \times 2048$, test mesh 256×4096) and $Ra = 10^{14}$ ($N_x \times N_z = 512 \times 4096$, test mesh 512×6144). In both cases, the discrepancies in Nusselt and Reynolds numbers remained below 1% and 4% respectively.

To reduce the calculation time, simulations were initialized using results from previous runs. Backward initialization tests were also performed to avoid subcritical or supercritical states near transition points. For comparison, additional simulations with uniform initialization (temperature $T = 0.5$ and velocity $\vec{u} = 0$) were carried out. The results of these comparisons will be discussed in the following section.

GLOBAL FLOW IN HIGH ASPECT RATIO

As outlined in the introduction, one of the central objectives of this study is to investigate the influence of an aspect ratio $\Gamma = 5$ on the three distinct regimes identified by Wang et al. (2021) These regimes are characterized as follows :

- **Regime I** : The vertical boundary layers remain fully laminar. A large scale convection loop is clearly defined, and the bulk region exhibits linear stratification out of the upper and lower boundary layers. In this regime, the central stratification $S = \left.\dfrac{\partial T}{\partial z}\right|_{center}$ is independent of the Rayleigh number.
- **Regime II** : Turbulent transition occurs within the boundary layers. The emergence of vortex structures on both side's corners generates homogeneous temperature zones, progressively displacing the isotherms toward the center of the bulk and enhancing stratification. As the Rayleigh number increases, turbulent regions extend toward the center of both plates. Jets from the hot and cold walls eventually converge, forming a well-mixed central region and reducing central stratification.
- **Regime III**: The well-mixed region expands further toward the upper and lower walls. Central stratification approaches zero and, once again, becomes independent of the Rayleigh number.

Our systematic results with higher aspect ratio confirm the same regime organization as depicted in figure 2, with transition mechanisms between regimes that are broadly similar. Specifically, the first Rayleigh number for which we observe turbulent development is about $Ra = 5 \times 10^{10}$, compared to the threshold $Ra_{I \to II} = 6 \times 10^{10}$ obtained in previous studies (Wang *et al.*, 2021*b*). This transition to turbulence is driven by the development of instabilities along the vertical plates. Given that the cavity height remains unchanged relative to the square case, one might anticipate similar transition criteria. The observed discrepancy could potentially be attributed to differences in top and bottom boundary conditions: a free surface may facilitate stronger recirculation in the corners, enhancing shear and promoting earlier instability development..

The primary effect of the aspect ratio lies in the evolution of the central stratification S in the regime II and the transition to regime III. The vortices first appear in the top left and bottom right corner, and then grow towards the center in a similar fashion as in the square cavity. The central stratification follows the same trend in both cases, with both homogeneous upper hot and lower cold regions pushing the isotherms towards the center. However, in the $\Gamma = 5$ case, the maximum will be reached sooner (at around $Ra = 4 \times 10^{11}$ versus $Ra = 7 \times 10^{11}$ in $\Gamma = 1$ case) , and S will decrease for a lower Rayleigh. The interpretation is that, for a narrower cavity as in our case, the plumes leaving the hot and cold plate will meet for a reduced intensity compared to the square case. This will lead to the growth of the central well-mixed area, and the early transition to the third regime (with a transition Rayleigh around $Ra = 10^{12}$ versus $Ra_{II \to III} \approx 5 \times 10^{12}$). As in the $\Gamma = 1$ case, S appears to plateau at the highest Rayleigh numbers.

To explore potential hysteresis effects, additional simulations were conducted for strongly stratified conditions ($Ra = 3 \times 10^{11}$, 5×10^{11} and 7×10^{11}), using uniform temperature ($T = 0.5$) and velocity ($\vec{u} = 0$) fields as initial conditions. The objective was to determine whether restarting from a pre-stratified state might yield stronger stratification. The results plotted on figure 2 showed no significant differences between the two initialization methods across the tested Rayleigh numbers. Eventual discrepancies could be attributed to incomplete convergence in the uniform-field simulations, as the extended transient phase increases computational time. Error bars were obtained by taking the minimum and maximum realization of the averaging for different sample sizes.

Other critical outputs analyzed in the study by Wang *et al.* (2021*b*) include the Nusselt number $Nu = \dfrac{hH}{\lambda}$ where h and λ represent the convective heat transfer coefficient and the thermal conductivity, respectively. Additionally, the wind-based Reynolds number is examined, defined as :

$$Re = \max_x \frac{\overline{w}H}{\nu},\ \overline{w} = \frac{1}{H} \int w(x,z)dz \qquad (2)$$

with ν the kinematic viscosity and $\overline{w}$ the mean profile along x of the vertical speed.
Their evolution with the Rayleigh is plotted with comparison to the result for $\Gamma = 1$ on figure 3. No discernible influence of the aspect ratio is observed on both quantities.The seamless continuity between Regime II and Regime III likely accounts for the absence of any evolution shift across the transition. The observed correlations remain consistent with the $\Gamma = 1$ case, namely :

- $Nu \propto Ra^{1/4}$ in the laminar region, $Nu \propto Ra^{1/3}$ in the turbulent one.
- $Re \propto Ra^{1/2}$ int the laminar region, $Re \propto Ra^{4/9}$ in the turbulent one.

BOUNDARY LAYER EVOLUTION

To quantify the global flow structures, we analyze the evolution of the averaged profile, both in time and over the vertical axis z in figure 4. For the temperature profile, as the Rayleigh number increases, the overall thermal boundary layer gets thinner. One can also notice a thin layer of return flow with temperature overshooting the mean temperature T=0.5 just outside the boundary layer. This overshoot phenomenon, quite pronounced in the laminar regime, decreases as turbulence develops and ultimately vanishes at the highest Rayleigh numbers. For the vertical velocity profile, we observe a similar trend up to $Ra = 5 \times 10^{11}$: the displacement boundary layer thins, and a thin layer with opposite sign velocity, initially present at low Rayleigh finally disappears. However, this trends stops once we reach the Rayleigh corresponding to the emergence of the central well-mixed region ($Ra = 4 \times 10^{11}$). At this stage, the boundary layer thickens due to the influence of turbulent structures. Concurrently, the location of the maximum vertical velocity shifts closer to the wall throughout the process, while its amplitude decreases. This reflects the increasing dissipation of kinetic energy within the turbulent flow structures.

We can quantify this evolution by introducing the thermal boundary thickness δ_{th} and the displacement thickness δ_{disp} as followed :

$$\delta_{th} = \int \frac{\overline{T}(x) - T_{bulk}}{T_{wall}} dx,\ \ \delta_{disp} = \int \frac{\overline{w}}{\max\limits_x \overline{w}} dx \qquad (3)$$

We can visualize the evolution of these two quantities, with the position of the velocity maximum along x, with respect to the Rayleigh as in figure 5. A well-documented effect in $Pr > 1$ fluids is that the thermal boundary layer is thinner than the viscous one. We assume that the thermal boundary layer would not be significantly affected by the transition to turbulence. This is confirmed by the plotted results, which remain close to the theoretical evolution $\delta_{th} \propto Ra^{-1/4}$ (Batchelor, 1954). The position of the velocity maxima seems to follow the same trend, keeping the scaling obtained in laminar regime even for high-Rayleigh simulation. This is consistent with the idea that this quantity can be representative of the viscous sub layer thickness, i.e. where the flow experiences the effect of the no-slip boundary condition,

On the other hand, the displacement thickness sees the transition to turbulence, as we depart from the $Ra^{-1/4}$ curve once we reach the regime II. It seems first to increase as the turbulence regions develop on both sides and merge in the center. Once fully in the regime III ($Ra > 10^{12}$), the displacement thickness stabilizes since, although the well mixed zone keeps extending towards the upper and lower region, it has little impact when averaging the vertical profiles.

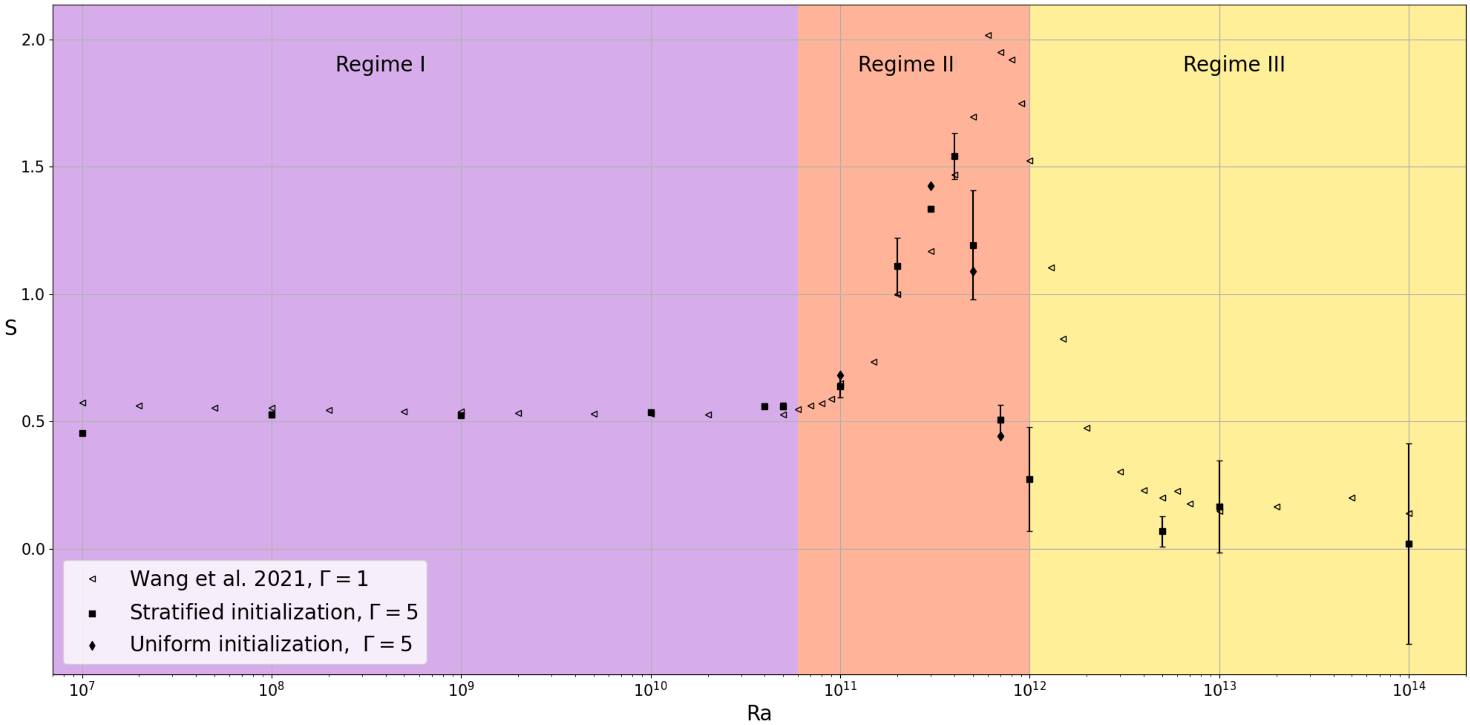

Figure 2. Evolution of the central stratification $S = \left.\frac{\partial T}{\partial z}\right|_{center}$ with respect to the Rayleigh number Ra. Results from Wang et al. (2021) in square cavities are plotted with empty triangles. Results from the current study are plotted in filled squares (initialization from the previous simulation) or filled diamonds (uniform start), with corresponding error bars.

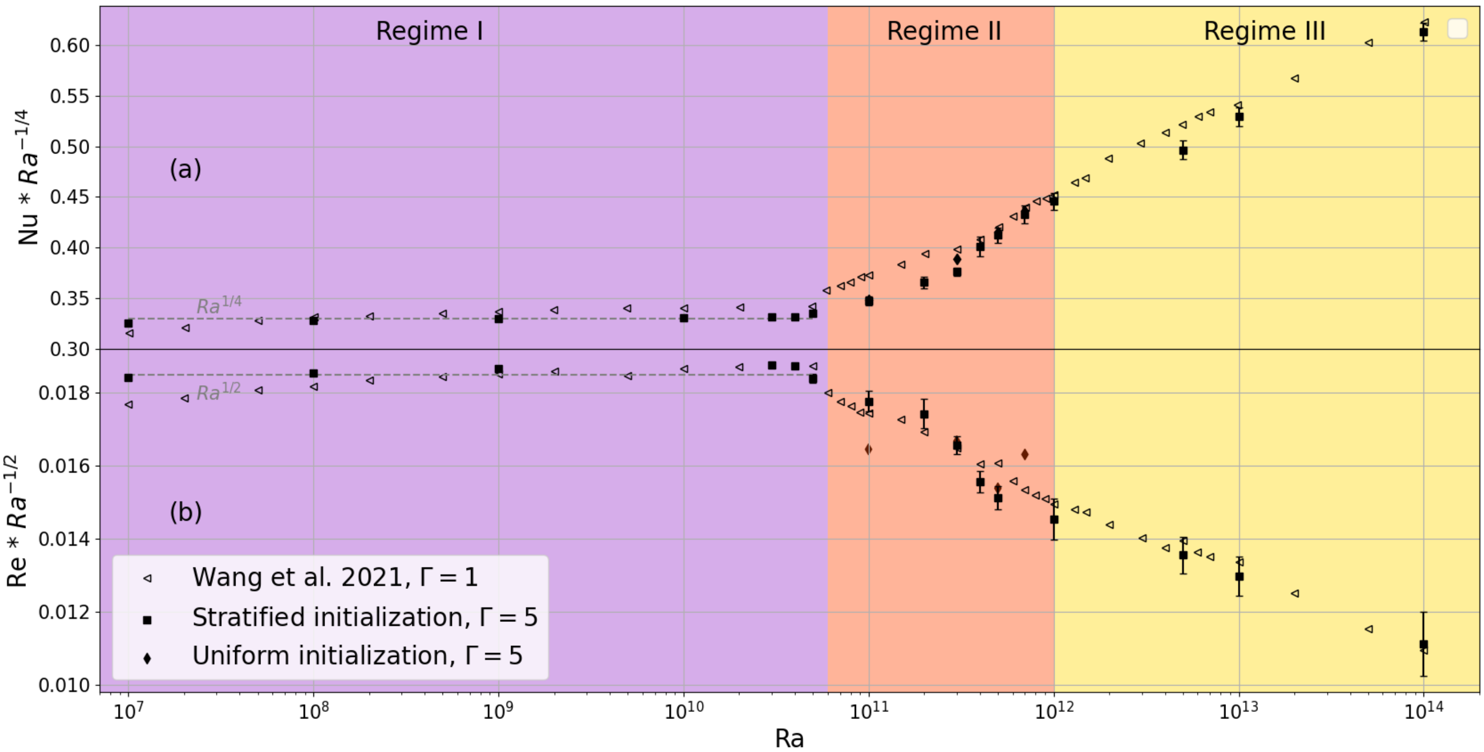

Figure 3. Evolution of the Nusselt number Nu and the Reynolds number Re with respect to the Rayleigh number, rescaled by $Ra^{1/4}$ and $Ra^{1/2}$ respectively. The legend is the same as in Figure 2.

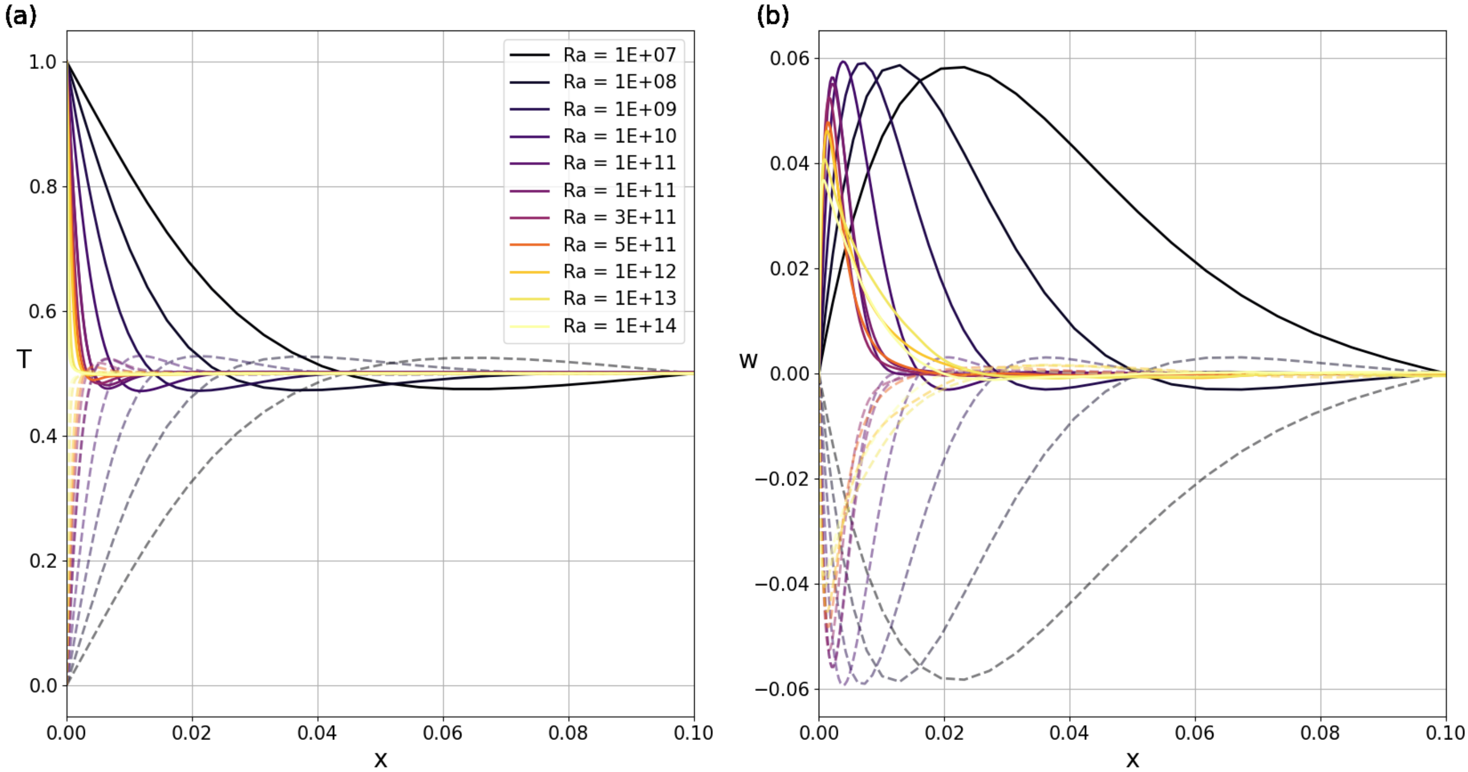

Figure 4. (a) Temperature T and (b) vertical velocity w profiles averaged in time and along z as a function of x for increasing Rayleigh numbers. Solid lines represent the left part of the profile, and dashed lines the right part folded back.

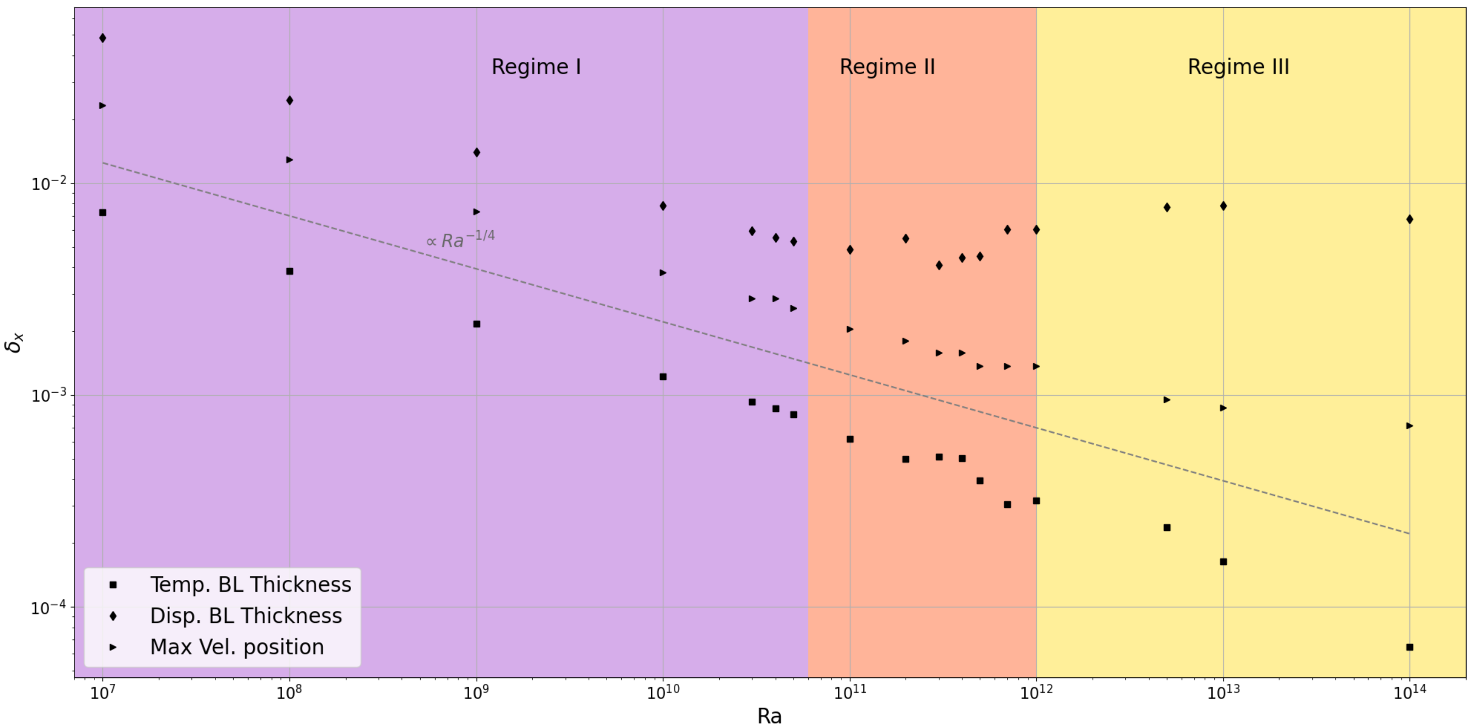

Figure 5. Evolution of the mean hot boundary thickness with respect to the Rayleigh number. Displacement thickness is represented with triangles, thermal thickness with squares and the position of vertical velocity maximum with diamonds. The $Ra^{-1/4}$ curve is also plotted with a dashed line.

CONCLUSION AND FUTURE WORK

This study examined the influence of a high aspect ratio $\Gamma = 5$ on the establishment of different vertical natural convection regimes previously identified in the literature in square geometries. Our results demonstrate that the transition from Regime I (laminar) to Regime II (turbulent) remains unaffected by the aspect ratio. However, the evolution of stratification, and thus the transition to regime III is significantly influenced by Γ. This transition is initiated by the formation of a well-mixed central zone, resulting from the convergence of hot and cold plumes leaving their respective walls. In a narrower cavity this convergence occurs at a comparatively lower convection intensity, thereby accelerating the transition to Regime III relative to the $\Gamma = 1$ case.

No significant deviations were observed in the evolution of the Nusselt and Reynolds numbers, confirming the scaling laws established by Wang *et al.* (2021*b*). This aligns with the previous observation that only the transition from laminar to turbulent regime affects these two global quantities.

A detailed analysis of the evolution of mean profiles and boundary layers helped us understand the underlying phenomenology. With increasing Rayleigh number, both thermal and viscous boundary layers thin, adhering to the scaling $Ra^{-1/4}$ suggested by Batchelor (1954). The displacement thickness follows the same trend until the onset of regime II, where the averaged contribution of the turbulent structures induces a thickening effect. In Regime III, this quantity stabilizes as turbulence dominates along the majority of both plates.

Next step should investigate the mechanisms by which turbulent structures control the mixing of isothermal layers and their evolution with the convection intensity. In particular, we aim to study the role of internal waves in the transition from regime II to III. Even if they are unlikely to be the primary driver, they are strongly coupled with stratification. This analysis could clarify how kinetic energy is redistributed as the maximum velocity amplitude decreases.

To further advance this work, exploring the effects of other aspect ratios, including $\Gamma < 1$ cases, would provide critical insights. As its effect was identified to be around the Regime II, a systematic study in this range of Rayleigh could provide further idea on how Γ will shift the maximum stratification.

Due to computational constraints, this study was conducted in 2D. The assumption was that the observed patterns closely approximate the 3D flow structure. Validation through 3D simulations is essential, albeit restricted to medium Rayleigh numbers. The additional boundaries conditions could create spurious structures that may affect the global flow dynamic (Sergent *et al.*, 2013*a*). This still will be a relevant range to study the stratification dynamic.

REFERENCES

Batchelor, G. K. 1954 Heat transfer by free convection across a closed cavity between vertical boundaries at different temperatures. *Quarterly of Applied Mathematics* **12** (3), 209–233.

Burns, Keaton J., Vasil, Geoffrey M., Oishi, Jeffrey S., Lecoanet, Daniel & Brown, Benjamin P. 2020 Dedalus: A flexible framework for numerical simulations with spectral methods. *Physical Review Research* **2** (2), 023068.

De Angelis, Alessandro, Reinke, Nils & Ambrosini, Walter 2023 Assessing water-wall behaviour for a light-water Small Modular Reactor with the aid of CFD analyses. *Annals of Nuclear Energy* **184**, 109672.

Ke, Junhao, Komiya, Atsuki, Armfield, Steven W. & Williamson, Nicholas John 2026 On the role of moderate Prandtl numbers in vertical natural convection. *Journal of Fluid Mechanics* **1029**, A37.

Khoubani, Arman, Mohanan, Ashwin Vishnu, Augier, Pierre & Flór, Jan-Bert 2024 Vertical convection regimes in a two-dimensional rectangular cavity: Prandtl and aspect ratio dependence. *Journal of Fluid Mechanics* **981**, A10.

Sergent, Anne, Joubert, Patrice, Xin, Shihe & Le Quéré, Patrick 2013*a* Resolving the stratification discrepancy of turbulent natural convection in differentially heated air-filled cavities Part II: End walls effects using large eddy simulation. *International Journal of Heat and Fluid Flow* **39**, 15–27.

Sergent, Anne, Xin, Shihe, Joubert, Patrice, Le Quéré, Patrick, Salat, Jacques & Penot, François 2013*b* Resolving the stratification discrepancy of turbulent natural convection in differentially heated air-filled cavities – Part I: Reference solutions using Chebyshev spectral methods. *International Journal of Heat and Fluid Flow* **39**, 1–14.

Trias, F.X., Gorobets, A., Soria, M. & Oliva, A. 2010 Direct numerical simulation of a differentially heated cavity of aspect ratio 4 with Rayleigh numbers up to 1011 – Part I: Numerical methods and time-averaged flow. *International Journal of Heat and Mass Transfer* **53** (4), 665–673.

Wang, Ben, Wang, Qi, Wan, Zhen-Hua & Sun, De-Jun 2021*a* The influence of aspect ratio on flow states in the buoyancy-driven turbulence with free slip boundaries. *International Journal of Heat and Mass Transfer* **178**, 121639.

Wang, Qi, Liu, Hao-Ran, Verzicco, Roberto, Shishkina, Olga & Lohse, Detlef 2021*b* Regime transitions in thermally driven high-Rayleigh number vertical convection. *Journal of Fluid Mechanics* **917**, A6.